BİTLİS EREN ÜNİVERSİTESİ
FEN BİLİMLERİ DERGİSİ

ISSN: 2147-3129 / e-ISSN: 2147-3188

Article Type	: Research Article	**Year**	: 2025
Received	: November 27, 2024	**Volume**	: 14
Revised	: February 2, 2025	**Issue**	: 1
Accepted	: February 5, 2025	**Pages**	: 385-397
DOI	: 10.17798/bitlisfen.1592320		

FLUOROQUINOLONE ANTIBIOTIC ADSORPTION ON THE FUNCTIONAL C_{70} FULLERENES: A COMPUTATIONAL INSIGHT ON ADSORBENT APPLICATIONS

İskender MUZ [1]

[1]*Nevşehir Hacı Bektaş Veli University, Faculty of Art and Sciences, Department of Physics, Nevşehir, Türkiye, iskender023@gmail.com*

ABSTRACT

Fluoroquinolone (FQ) adsorption on functional (Ca-, Fe-, Mg- and Zn-doped) C_{70} fullerenes was investigated for the first time by density functional theory (DFT). Mg, Ca, Fe, and Zn doping were found to enhance sensitivity to FQ. The adsorption energies of functional C_{70} fullerenes after FQ adsorption were found in the range of 23-37 kcal/mol. UV-Visible analysis reveals that the absorption maximum of the doped C_{70} fullerenes shifts to a longer wavelength after the FQ adsorption. Moreover, the FQ adsorption significantly lowered the LUMOs in the Fe-doped C_{70} fullerene. The Fe-doped C_{70} fullerene also caused a notable decrease in band gap energy after FQ adsorption. Thus, Fe doping significantly increased the electrical conductivity, enabling the detection of FQ antibiotic on C_{70} fullerene. The results revealed that Fe-doped C_{70} fullerene may be a suitable adsorbent for FQ antibiotic.

Keywords: DFT, Fullerenes, Fluoroquinolone, Adsorbent.

1 INTRODUCTION

Fluoroquinolones (FQs) are a family of broad-spectrum antibiotics widely utilized to treat a various bacterial infections involving respiratory tract infections, urinary tract infections, gastrointestinal infections, and some skin infections [1], [2]. Through environmental factors such as agricultural runoff and wastewater irrigation, the FQs can penetrate and accumulate in the soil. Moreover, the FQs can persist for long periods of time after interaction with soil due to their low biodegradability. As a result, disruption of the soil microbiome can lead to various

environmental and health problems such as antibiotic resistance, plant uptake, and bioaccumulation in soil organisms [3], [4], [5], [6].

In recent decades, research has concentrated on examining the effectiveness of various adsorbent materials, such as activated carbon, clay minerals, ion exchange resins, and biochar, for removing fluoroquinolones [6], [7], [8]. However, most of these materials have some problems, such as high price and low adsorption ability [9], [10]. Therefore, there is a need for both low-cost and effective adsorbents to remove the FQs from contaminated environment.

Fullerenes are investigated for a variety of applications, including drug delivery, storage and adsorbents due to their unique structure and chemical stability. Furthermore, many studies shown that functional fullerenes can enhance their adsorption capacity and carrier properties [11], [12], [13], [14], [15], [16], [17], [18], [19], [20], [21], [22], [23]. N- and B-doped C_{70} fullerenes increase the sensitivity to mercaptopurine [24] and enhance the adsorption ability of pyrazinamide [25]. Al doping increases the adsorption ability of both C_{60} and C_{70} fullerenes, leading to stronger and more stable interactions with gemcitabine [26]. The Si- and Al-doped C_{70} fullerenes can effective materials for amphetamine detecting in various applications including drug monitoring and law enforcement [27]. This is due to changes in electronic properties that improve the binding interaction between drugs and functional C_{70} fullerenes. However, no study has specifically investigated the interaction between C_{70} fullerenes and the FQ antibiotic. Moreover, functional C_{70} fullerenes could be effective materials for detecting the FQ in various applications, including cancer therapy, drug administration and adsorbents. The purpose of study is to examine the possibility of the use of functional C_{70} fullerenes as an adsorbent to detect the FQ. The results including adsorption energies, HOMO – LUMO energy gaps, DOS, UV-visible absorption spectra and reactivity properties of pristine, Ca-, Fe-, Mg- and Zn-doped C_{70} fullerenes are examined by DFT/TD-DFT calculations [28].

2 COMPUTATIONAL DETAILS

Density functional calculations are carried out using Gaussian 09 software [29] on pristine, Ca-, Fe-, Mg- and Zn-doped C_{70} fullerenes, employing the B3LYP functional, 6-311G(d,p) basis set [30], and Grimme's three-parameter (GD3) empirical dispersion correction [31]. The density of spectra (DOS) are generated using GaussSum program [32]. Adsorption energies (E_{ad}) are generated by following equation:

$$E_{ad} = E\left(\frac{FQ}{Fullerenes}\right) - E(Fullerenes) - E(FQ) + E(BSSE) \quad (1)$$

where BSSE is taken into consideration in the study because it produces accurate results in the calculation of weak interactions. Furthermore, the chemical hardness (η), chemical potential (μ), electrophilicity index (ω) and maximum amount of electronic charge index (ΔN_{tot}) are calculated from Koopman's theorem [33] using HOMO and LUMO energies as following: $\eta = (I - A)/2$, $\omega = \mu^2/2\eta$ and $\Delta N_{tot} = -\mu/\eta$. Multiwfn [34] and VMD [35] softwares used to calculate noncovalent interactions (NCI) and reduced density gradient (RDG). Additionally, TD-DFT calculations using the CAM-B3LYP functional [36] with the 6-311G(d,p) basis set are conducted to predict the UV-Vis absorption spectra.

3 RESULTS AND DISCUSSION

Figure 1 shows the electrostatic potential (ESP) patterns of the FQ and pristine C_{70} fullerene. The ESP is a quantity that reflects the potential energy stored in the field. Blue color show electro positivity, indicating that there is correlated with electron poor, while red color is presented for evaluation of electro negativity, indicating electron rich area (see Figure 1). The O and F atom of the FQ antibiotic is electron rich sites (in range of -0.02 – -0.03 a.u.). Since the O atom of FQ has a higher electronegativity than N, the electrostatic potential near O atom is stronger or more negative than near N atom. Moreover, the pristine C_{70} fullerene has a more neutral ESP pattern than FQ antibiotic.

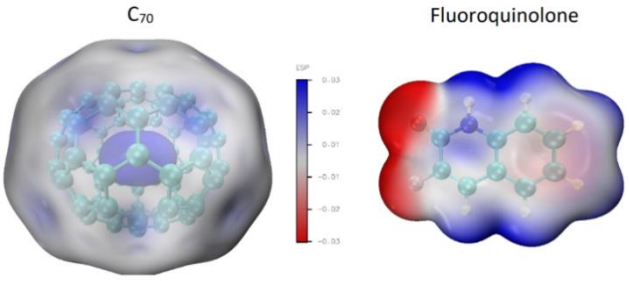

Figure 1. ESP patterns of pristine C_{70} fullerene (left) and FQ antibiotic (right).

The ESP patterns of functional C_{70} fullerene have been presented in Figure 2. The Ca, Fe, Mg and Zn doping to C_{70} fullerenes increases electronegativity by making the complex electron-rich, enhancing bonding capabilities. The functional C_{70} fullerenes with increased electronegativity may be more prone to interact with FQ. Therefore, functional C_{70} fullerenes result in stronger electron attraction of FQ antibiotic compared to pristine ones. In this study,

the results are investigated for electron transfers between functionalized C_{70} fullerenes and FQ which includes the electrons of red region (see Figure 2).

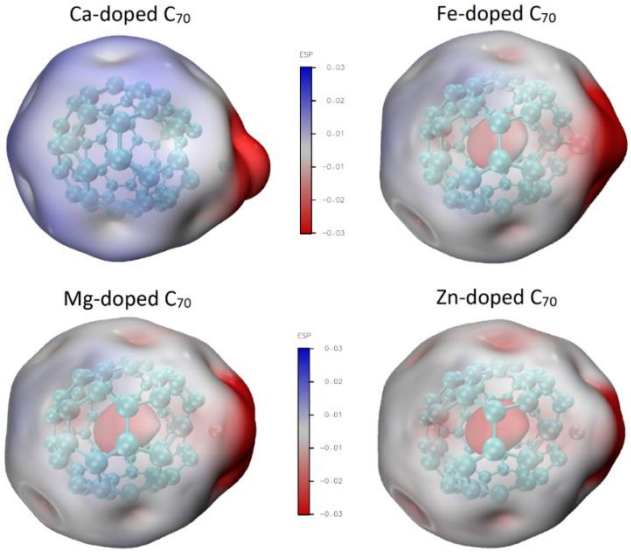

Figure 2. ESP patterns of functional C_{70} fullerenes.

Figure 3 shows the frontier molecular orbital analysis for FQ adsorption on pristine, Ca, Fe-, Mg- and Zn-doped C_{70} fullerenes.

Table 1. The calculated electronic parameters for pristine and functional C_{70} fullerenes before and after FQ adsorption.

Structure	E_g (eV)	LUMO (eV)	HOMO (eV)	ΔE_g	E_{ad} (kcal/mol)
C_{70}	2.68	-3.66	-6.34	-	-
C_{70}-FQ	2.69	-3.56	-6.25	0.37	-0.87
CaC_{70}	1.51	-4.00	-5.51	-	-
CaC_{70}-FQ	1.50	-3.47	-4.97	-0.66	-29.89
FeC_{70}	1.98	-3.88	-5.86	-	-
FeC_{70}-FQ	1.86	-3.40	-5.26	-6.06	-37.14
MgC_{70}	1.57	-4.33	-5.90	-	-
MgC_{70}-FQ	1.61	-3.64	-5.25	2.55	-34.42
ZnC_{70}	1.58	-4.49	-6.07	-	-
ZnC_{70}-FQ	1.65	-3.78	-5.43	4.43	-23.26

Frontier molecular orbital analysis helps to understand charge transfer processes by examining the interactions between the highest occupied molecular orbital (HOMO) of one molecule and the lowest unoccupied molecular orbital (LUMO) of another, which determines the ease and direction of electron transfer in a reaction. E_g values decreased in all the heterofullerenes after Ca and Fe, Mg and Zn doping was applied and electrical conductivity increased when compared to the pristine C_{70} fullerene results. The E_g values after Ca, Fe, Mg and Zn doping are found to be in the following decreasing order: pristine (2.68 eV) > Fe- (1.98

eV) > Zn- (1.58 eV) > Mg- (1.57 eV) > Ca- (1.51 eV). The E_g values of Ca- and Fe-doped C_{70} fullerenes before and after FQ adsorption are decreased, but Mg- and Zn-doped C_{70} fullerenes are increased (see Table 1). The percentage of difference of the HOMO-LUMO energy gap (ΔE_g) of complexes before and after FQ adsorption are shown in Figure 3. The ΔE_g values of Ca- and Fe-doped C_{70} fullerenes are slightly decreased in the range of 0.66 % and 6.06 %, but Mg- and Zn-doped C_{70} fullerenes are increased in the range of 2.55 % and 4.43 %. These results show that Ca and Fe doping and FQ adsorption increase electrical conductivity. Furthermore, Fe-doped C_{70} fullerene could be a suitable candidate for FQ adsorbents.

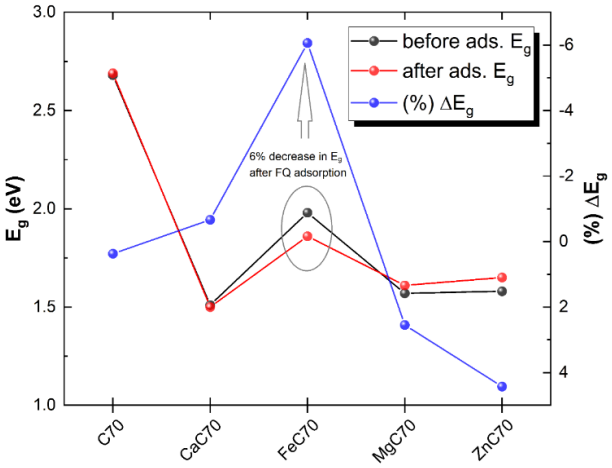

Figure 3. E_g and ΔE_g graphs before and after FQ adsorption.

Figure 4 shows the E_{ad} graph after FQ adsorption. Adsorption energy (E_{ad}) indicates to the energy change when a FQ antibiotic attaches to surface of a C_{70} fullerene. The E_{ad} values of pristine C_{70} fullerene is calculated to be -0.87 kcal mol^{-1}, indicating very low adsorption capacity. However, the E_{ad} drops sharply after Ca and Fe, Mg and Zn doping and it is calculated to be in the range of -29.89 and -37.14 kcal/mol.

Table 2. The calculated reactivity parameters for pristine and functional C_{70} fullerenes before and after FQ adsorption.

Structure	η (eV)	μ (eV)	ω (eV)	ΔN_{tot} (eV)
C_{70}	1.34	-5.00	9.33	3.73
C_{70}-FQ	1.35	-4.91	8.94	3.65
CaC_{70}	0.76	-4.76	14.97	6.30
CaC_{70}-FQ	0.75	-4.22	11.87	5.63
FeC_{70}	0.99	-4.87	11.98	4.92
FeC_{70}-FQ	0.93	-4.33	10.08	4.66
MgC_{70}	0.79	-5.12	16.66	6.52
MgC_{70}-FQ	0.81	-4.45	12.27	5.52
ZnC_{70}	0.79	-5.28	17.64	6.68
ZnC_{70}-FQ	0.83	-4.61	12.85	5.58

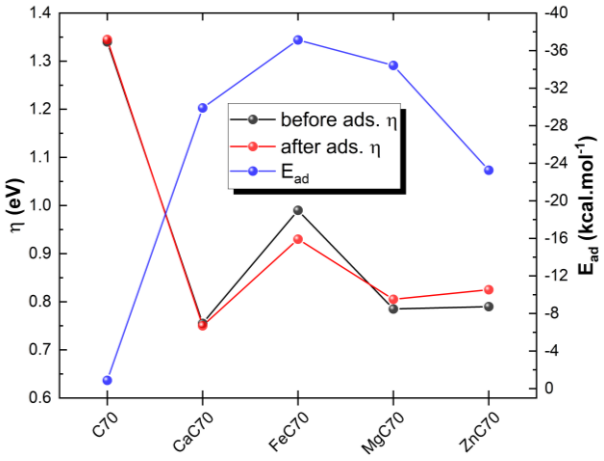

Figure 4. E_{ad} and η graphs for before and after FQ adsorption.

Table 2 lists quantum molecular descriptors, which are computational parameters derived from quantum chemical calculations that provide insights into a system's electronic structure, reactivity, stability, and interactions, helping predict chemical behavior and properties in various molecular systems. The chemical hardness (η) is described as a measure of a system's resistance to changes in its electron density. The η graph for before and after FQ is shown in Figure 4. After FQ adsorption, Fe-doped C_{70} fullerene has the highest hardness value (see Table 1). η value after both doping and adsorption is calculated to be in the following decreasing order: Fe- (0.93 eV) > Zn- (0.83 eV) > Mg- (0.81 eV) > Ca- (0.75 eV). This is followed by the fact that the electrophilic index (ω) and electronic charge index (ΔN_{tot}) seen in Table 2 have relatively lower values compared to the other doped (Ca, Mg and Zn) atoms. After FQ adsorption, Ca-doped C_{70} fullerene has the lowest hardness value. In other words, this is an indication that the complex is softer. Therefore, Ca-doped C_{70} fullerene is more reactive and can interact more strongly with the surfaces compared to the other dopant atoms. Comparing the graphs in Figure 4, after FQ adsorption, Fe-doped C_{70} fullerene has the highest hardness and adsorption energy. This may indicate that Fe-doped C_{70} fullerene binds to the FQ antibiotic by physical adsorption. In addition, Ca-doped C_{70} fullerene can bind to FQ antibiotic with stronger physical adsorption compared to Fe-doped C_{70} fullerene. For more detailed analysis of HOMO and LUMO changes of all complexes (CaC_{70}-FQ, FeC_{70}-FQ, MgC_{70}-FQ and ZnC_{70}-FQ) before and after FQ adsorption, DOS graphs were drawn and presented in Figures 5–6. HOMO and LUMO energies give insights into a molecule's electron-donating ability and electron-accepting ability, respectively. In addition, the energies of HOMO and LUMO are crucial in understanding the electronic character of complexes, reactivity, and its ability to absorb light.

Figure 5 shows the DOS plots of the doped (Ca, Fe, Mg and Zn) atoms compared to the pristine C_{70} fullerene in the range of -8.0-0.0 eV. The atoms doped to pristine C_{70} fullerene increase the HOMO value (see Table 1). Therefore, it is seen that the electron-donating tendency and electron-donating capacity of fullerenes increase after doping. The HOMO value of pristine C_{70} fullerene is calculated as -6.34 eV. The increase in HOMO values is found to be in the following decreasing order: Ca- (-5.51 eV) > Fe- (-5.86 eV) > Zn- (-5.90 eV) > Mg- (-6.07 eV). After doping, the HOMO value of Ca doped C_{70} fullerene is the highest and has increased from -6.34 to -5.51 eV compared to the pristine one. For this reason, the highest electron donation desire occurred with Ca doping and the lowest electron donation desire occurred with Mg doping. The LUMO value of pristine C_{70} fullerene is calculated as -3.66 eV. The decrease in LUMO values is found to be in the following increasing order: Ca- (-3.88 eV) < Ca- (-4.00 eV) < Mg- (-4.33 eV) < Zn- (-4.49 eV). After doping, the LUMO value of Ca doped C_{70} fullerene is the lowest and has decreased from -3.66 to -3.88 eV compared to the pristine one. Thus, the highest electron acceptance willingness has occurred with Fe doping.

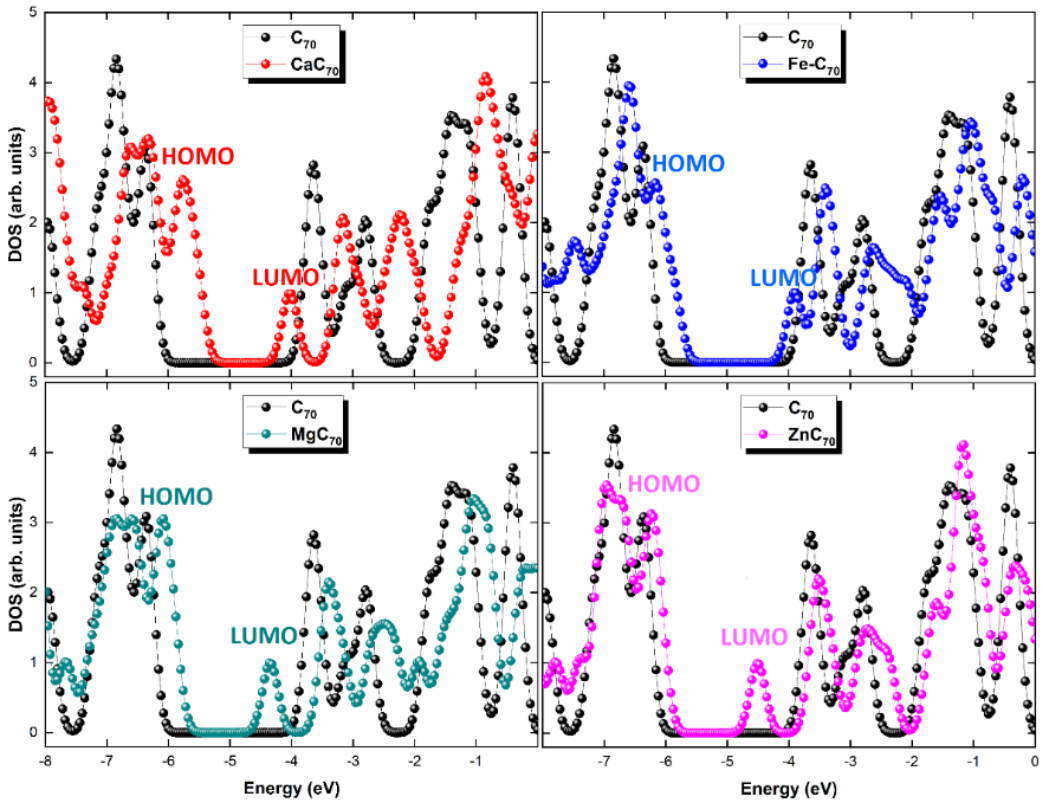

Figure 5. DOS of pristine and functionalized C_{70} fullerenes before FQ adsorption.

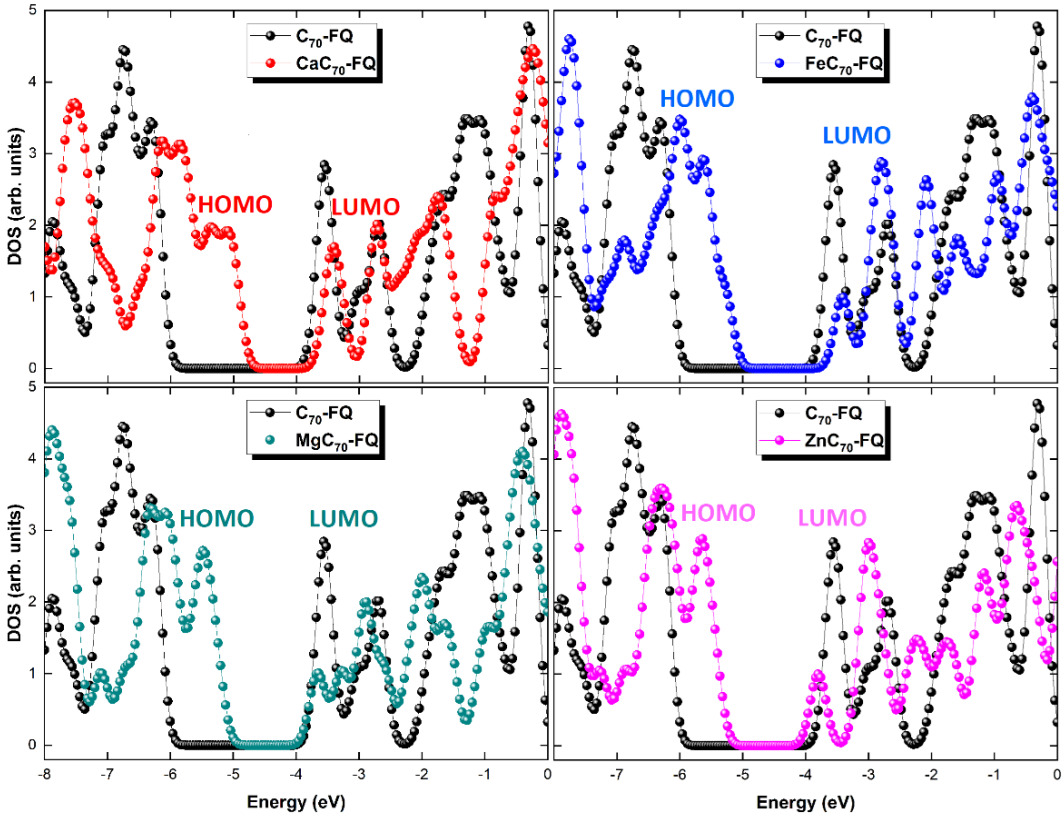

Figure 6. DOS of pristine and functionalized C_{70} fullerenes after FQ adsorption.

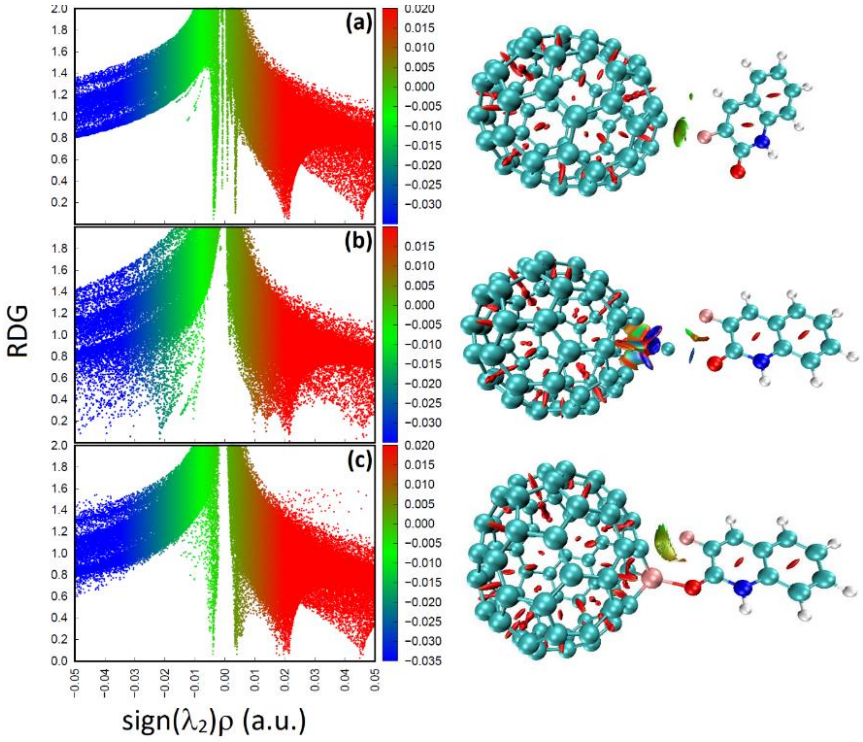

Figure 7. RDG plots and NCI isosurfaces of (a) pristine, (b) Ca- and (c) Fe-doped C_{70} fullerenes after FQ adsorption.

Figure 6 shows the DOS graphs of CaC_{70}-FQ, FeC_{70}-FQ, MgC_{70}-FQ and ZnC_{70}-FQ complexes compared to pristine C_{70} fullerene after FQ adsorption (C_{70}-FQ). HOMO values increase after doping and FQ adsorption (see Table 1). The HOMO value of C_{70}-FQ complex is calculated as -6.25 eV. The increase in HOMO values is found to be in the following decreasing order: Zn- (-5.43 eV) > Fe- (-5.26 eV) > Mg- (-5.25 eV) > Mg- (-4.97 eV). The decrease in LUMO values is calculated to be in the following decreasing order: Fe- (-3.40 eV) > Ca- (-3.47 eV) > Mg- (-3.64 eV) > Mg- (-3.78 eV). After FQ adsorption, the LUMO value of Fe doped C_{70} fullerene is the lowest and has decreased from -3.56 to -3.40 eV compared to the pristine one (see Table 1). Thus, the highest electron acceptance willingness has occurred with both Fe doping and FQ adsorption.

When the E_g, ΔE_g and DOS values are examined, NCI and RDG analyses for two promising complexes (Ca- and Fe-doped C_{70} fullerene) are presented in Figure 7. Low and high RDG values are represented by the blue color (electrostatic attraction) and red color (electrostatic repulsive), respectively. Furthermore, green color indicates regions with intermediate RDG values. These can represent places where noncovalent interactions are neither particularly strong nor weak. This could correspond to weak dipole-dipole interactions or Van der Waals forces. When RDG and NCI analyses are examined, it is seen that Ca-doped C_{70} fullerene is in a stronger electrostatic attraction region to FQ antibiotic compared to Fe-doped C_{70} fullerene. This supports that Ca-doped C_{70} fullerene has a stronger physical adsorption compared to Fe-doped C_{70} fullerene.

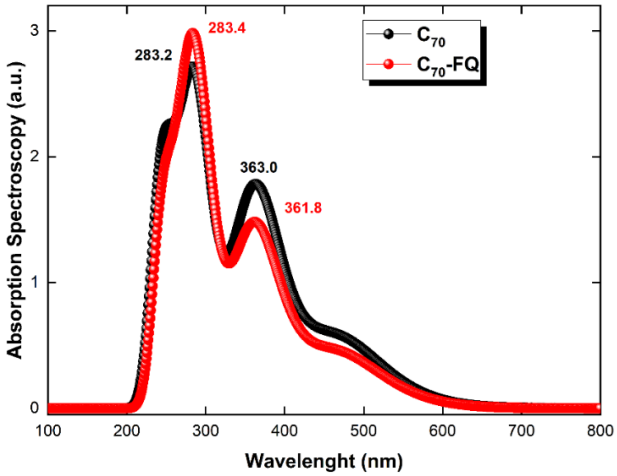

Figure 8. UV spectra of pristine C_{70} fullerene before and after FQ adsorption.

Figures 8–9 show the UV–vis absorption spectra of pristine and functionalized C_{70} fullerenes before and after FQ adsorption, respectively. The UV–vis absorption spectra provide information about the light of absorption of the system in the ultraviolet (UV) and visible (vis) regions of the electromagnetic spectrum before and after FQ adsorption. The adsorption spectrum of pristine C_{70} fullerene shows a peak at 283.2 nm. After FQ adsorption, it showed a sharply peak at 283.4 nm with a very small shift (see Figure 8). Furthermore, it indicates that small changes occur in the pristine C_{70} fullerene environment without a major structural change or strong chemical reaction in the C_{70}-FQ complex. After FQ adsorption with Ca, Fe, Mg and Zn doping, the CaC_{70}-FQ, FeC_{70}-FQ, MgC_{70}-FQ and ZnC_{70}-FQ complexes show peaks at 283.6 nm, 290.4 nm, 281.6 nm and 276.8 nm, respectively (see Figure 9). In the Ca, Fe, Mg, and Zn-doped C_{70} complexes, the wavelength of the absorption maximum is shifted to a longer value after FQ adsorption. This serves as a clear indication of the alteration in the energy levels of the complex resulting from the interaction between FQ and doped C_{70} fullerenes. Furthermore, the shift of the maximum wavelength of Fe-doped C_{70} fullerene from 277.6 nm to 290.4 nm after FQ adsorption represents the largest shift compared to the others. It should also be noted that the strongest interaction may occur between Fe-doped C_{70} fullerene and FQ.

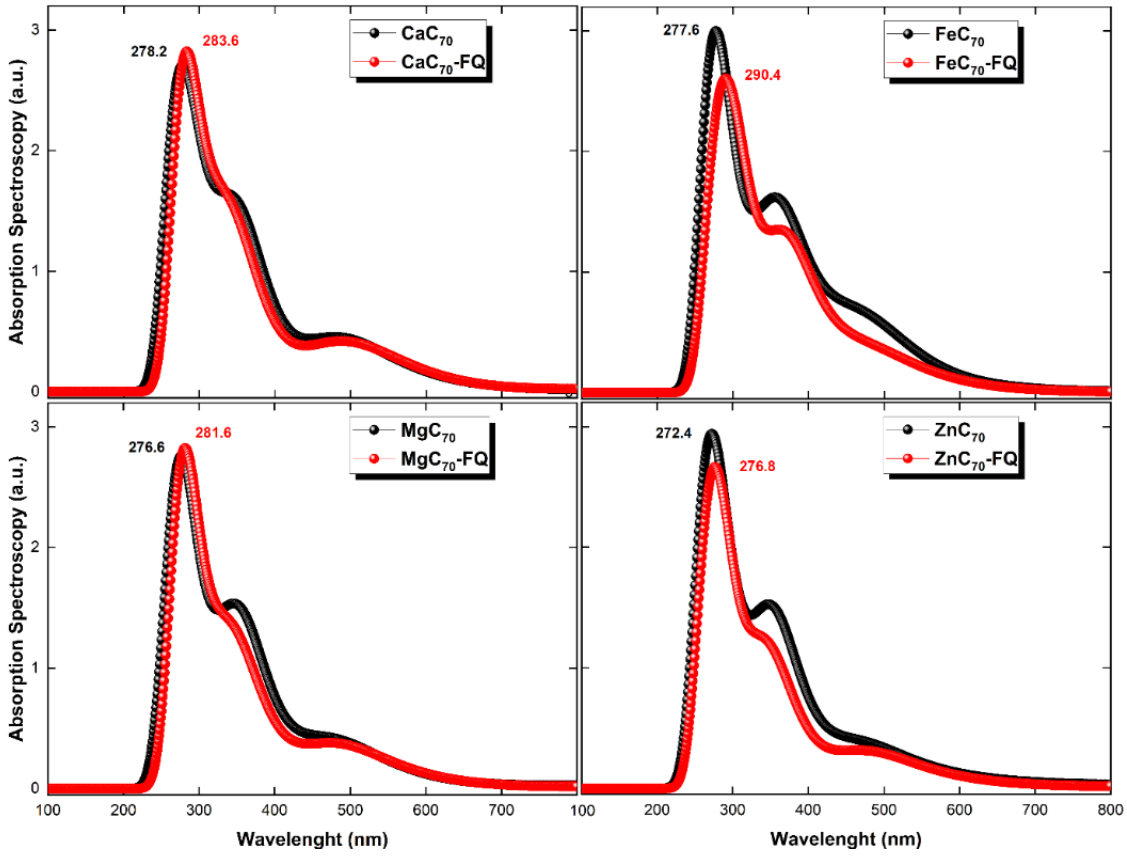

Figure 9. UV spectra of functionalized C_{70} fullerenes before and after FQ adsorption.

4 CONCLUSIONS

The adsorption of FQ antibiotic on the surface of four different functional C_{70} fullerenes has been examined using the DFT and TD-DFT methods. The FQ antibiotic is adsorbed onto the pristine C_{70} fullerene through its O-head, with an adsorption energy of around -0.87 kcal/mol. When the C atom of C_{70} is replaced by Ca, Fe, Mg and Zn atoms, adsorption energies increase and reach values between -23.26 and -37.14 kcal/mol. Time-dependent DFT calculations show that the absorption spectra of FQ/fullerene complexes shift toward higher wavelengths. The RDG and NCI analyses indicate that Ca-doped C_{70} fullerene exhibits a stronger region of electrostatic attraction to the FQ antibiotic compared to Fe-doped C_{70} fullerene. Ca, Fe, Mg and Zn doping causes small changes in HOMO and LUMO energies of functional C_{70} fullerenes. When the percentage values of the difference in band gap energies are compared, however, the electrical conductivity is significantly increased after FQ adsorption with Fe doping, which can enable the detection of FQ antibiotic on functional C_{70} fullerene. Fe-doped C_{70} fullerene causes a significant decrease in band gap energy after FQ adsorption. Thus, an increase in electrical conductivity occurs and an electrical signal can be generated. Furthermore, UV-Vis absorption spectra clearly indicate that the strongest interaction would be between Fe-doped C_{70} fullerene and FQ. The results of this study suggest that Fe-doped C_{70} fullerene may be a better adsorbent for FQ antibiotic.

Acknowledgment

The numerical calculations reported were partially performed at TUBITAK ULAKBIM, High Performance and Grid Computing Centre (TRUBA resources), Türkiye.

Statement of Research and Publication Ethics

The study is complied with research and publication ethics.

Artificial Intelligence (AI) Contribution Statement

This manuscript was entirely written, edited, analyzed, and prepared without the assistance of any artificial intelligence (AI) tools. All content, including text, data analysis, and figures, was solely generated by the author.

REFERENCES

[1] Y. Xiang *et al.*, "Fabrication of sustainable manganese ferrite modified biochar from vinasse for enhanced adsorption of fluoroquinolone antibiotics: Effects and mechanisms," *Sci. Total Environ.*, vol. 709, p. 136079, Mar. 2020.

[2] S.-H. Chang, C.-C. Lu, C.-W. Lin, K.-S. Wang, M.-W. Lee, and S.-H. Liu, "Waste expanded polystyrene modified with H2SO4/biodegradable chelating agent for reuse: As a highly efficient adsorbent to remove fluoroquinolone antibiotic from water," *Chemosphere*, vol. 288, p. 132619, Feb. 2022.

[3] X. Liu, S. Lu, W. Guo, B. Xi, and W. Wang, "Antibiotics in the aquatic environments: A review of lakes, China," *Sci. Total Environ.*, vol. 627, pp. 1195–1208, Jun. 2018.

[4] X. Chi *et al.*, "Influent characteristics affect biodiesel production from waste sludge in biological wastewater treatment systems," *Int. Biodeterior. Biodegradation*, vol. 132, pp. 226–235, Aug. 2018.

[5] X. Van Doorslaer, J. Dewulf, H. Van Langenhove, and K. Demeestere, "Fluoroquinolone antibiotics: An emerging class of environmental micropollutants," *Sci. Total Environ.*, vol. 500–501, pp. 250–269, Dec. 2014.

[6] J. Kurasam, P. Sihag, P. K. Mandal, and S. Sarkar, "Presence of fluoroquinolone resistance with persistent occurrence of gyrA gene mutations in a municipal wastewater treatment plant in India," *Chemosphere*, vol. 211, pp. 817–825, Nov. 2018.

[7] S. A. C. Carabineiro, T. Thavorn-Amornsri, M. F. R. Pereira, and J. L. Figueiredo, "Adsorption of ciprofloxacin on surface-modified carbon materials," *Water Res.*, vol. 45, no. 15, pp. 4583–4591, 2011.

[8] Q. Wu, Z. Li, H. Hong, K. Yin, and L. Tie, "Adsorption and intercalation of ciprofloxacin on montmorillonite," *Appl. Clay Sci.*, vol. 50, no. 2, pp. 204–211, Oct. 2010.

[9] M. E. Peñafiel, J. M. Matesanz, E. Vanegas, D. Bermejo, R. Mosteo, and M. P. Ormad, "Comparative adsorption of ciprofloxacin on sugarcane bagasse from Ecuador and on commercial powdered activated carbon," *Sci. Total Environ.*, vol. 750, p. 141498, Jan. 2021.

[10] X. Peng, F. Hu, T. Zhang, F. Qiu, and H. Dai, "Amine-functionalized magnetic bamboo-based activated carbon adsorptive removal of ciprofloxacin and norfloxacin: A batch and fixed-bed column study," *Bioresour. Technol.*, vol. 249, pp. 924–934, Feb. 2018.

[11] E. S. Mirkamali, R. Ahmadi, K. Kalateh, and G. Zarei, "Adsorption of melphalan anticancer drug on the surface of fullerene (C-24): a comprehensive DFT study," *NANOMEDICINE J.*, vol. 6, no. 2, pp. 112–119, 2019.

[12] L. Zhang, Y.-L. Ye, X.-H. Li, J.-H. Chen, and W.-M. Sun, "On the potential of all-boron fullerene B40 as a carrier for anti-cancer drug nitrosourea," *J. Mol. Liq.*, vol. 342, p. 117533, Nov. 2021.

[13] C. Parlak and Ö. Alver, "A density functional theory investigation on amantadine drug interaction with pristine and B, Al, Si, Ga, Ge doped C60 fullerenes," *Chem. Phys. Lett.*, vol. 678, pp. 85–90, 2017.

[14] S. Bagheri Novir and M. R. Aram, "Quantum mechanical simulation of Chloroquine drug interaction with C60 fullerene for treatment of COVID-19," *Chem. Phys. Lett.*, vol. 757, p. 137869, Oct. 2020.

[15] F. Nattagh, S. Hosseini, and M. D. Esrafili, "Effects of B and N doping/codoping on the adsorption behavior of C60 fullerene towards aspirin: A DFT investigation," *J. Mol. Liq.*, vol. 342, p. 117459, Nov. 2021.

[16] İ. Muz, F. Göktaş, and M. Kurban, "A density functional theory study on favipiravir drug interaction with BN-doped C60 heterofullerene," *Phys. E Low-dimensional Syst. Nanostructures*, vol. 135, p. 114950, Jan. 2022.

[17] İ. Muz and M. Kurban, "A first-principles evaluation on the interaction of 1,3,4-oxadiazole with pristine and B-, Al-, Ga-doped C60 fullerenes," *J. Mol. Liq.*, vol. 335, p. 116181, 2021.

[18] İ. Muz, "Enhanced adsorption of fluoroquinolone antibiotic on the surface of the Mg-, Ca-, Fe- and Zn-doped C60 fullerenes: DFT and TD-DFT approach," *Mater. Today Commun.*, vol. 31, p. 103798, Jun. 2022.

[19] W. Li and T. Zhao, "Hydroxyurea anticancer drug adsorption on the pristine and doped C70 fullerene as potential carriers for drug delivery," *J. Mol. Liq.*, vol. 340, p. 117226, Oct. 2021.

[20] S. Onsori and S. Montazeri, "Pyrazinamide Drug Adsorption on the Pristine and Doped C70 Fullerenes: A DFT/TDDFT Study," *J. Inorg. Organomet. Polym. Mater.*, vol. 31, no. 11, pp. 4222–4235, Nov. 2021.

[21] A. S. Ghasemi, F. Ashrafi, S. A. Babanejad, and A. Elyasi, "Study of the Physicochemical Properties of Anti-Cancer Drug Gemcitabine on the Surface of Al Doped C60 and C70 Fullerenes: A DFT Computation," *J. Struct. Chem.*, vol. 60, no. 1, pp. 13–19, Jan. 2019.

[22] W. Liu, J. Wei, and Y. Chen, "Electrospun poly(L-lactide) nanofibers loaded with paclitaxel and water-soluble fullerenes for drug delivery and bioimaging," *New J. Chem.*, vol. 38, no. 12, pp. 6223–6229, Nov. 2014.

[23] M. K. Kiani, A. S. Ghasemi, and F. Ravari, "Theoretical study on carbonaceous materials as high efficient carriers for crizotinib drug in liquid water by density functional theory approach," *Struct. Chem.*, vol. 31, no. 4, pp. 1553–1561, Aug. 2020.

[24] Y. Yang, A. Sun, and W. Gu, "Sensing behavior of pristine and doped C70 fullerenes to mercaptopurine drug: a DFT/TDDFT investigation," *Struct. Chem.*, vol. 32, no. 1, pp. 457–468, Feb. 2021.

[25] S. Onsori and S. Montazeri, "Pyrazinamide Drug Adsorption on the Pristine and Doped C70 Fullerenes: A DFT/TDDFT Study," *J. Inorg. Organomet. Polym. Mater.*, vol. 31, no. 11, pp. 4222–4235, Nov. 2021.

[26] A. S. Ghasemi, F. Ashrafi, S. A. Babanejad, and A. Elyasi, "Study of the Physicochemical Properties of Anti-Cancer Drug Gemcitabine on the Surface of Al Doped C60 and C70 Fullerenes: A DFT Computation," *J. Struct. Chem.*, vol. 60, no. 1, pp. 13–19, 2019.

[27] E. Alipour, S. Maleki, N. Razavipour, N. Hajali, and S. Jahani, "Identification of amphetamine as a stimulant drug by pristine and doped C70 fullerenes: a DFT/TDDFT investigation," *J. Mol. Model.*, vol. 27, no. 6, p. 169, Jun. 2021.

[28] M. Özcan, A. K. Havare, İ. Dervişoğlu, and Z. Yegingil, "DFT-based simulation for the semiconductor behavior of XGeCl3 (X=K, Rb) halide perovskites under hydrostatic pressure," *Phys. Scr.*, vol. 99, no. 10, p. 105914, Sep. 2024, doi: 10.1088/1402-4896/AD7243.

[29] M. J. Frisch *et al.*, "Gaussian 09, Revision E.01," 2009.

[30] A. D. Becke, "A new mixing of hatree-fock and local density functional theories," *J. Chem. Phys.*, vol. 98, no. 2, pp. 1372–1377, Jan. 1993.

[31] S. Grimme, S. Ehrlich, and L. Goerigk, "Effect of the Damping Function in Dispersion Corrected Density Functional Theory," *J. Comput. Chem.*, vol. 32, no. 7, pp. 1456–1465, May 2011.

[32] N. M. O'Boyle, A. L. Tenderholt, and K. M. Langner, "cclib: A library for package-independent computational chemistry algorithms," *J. Comput. Chem.*, vol. 29, no. 5, pp. 839–845, 2008.

[33] T. Koopmans, "Über die Zuordnung von Wellenfunktionen und Eigenwerten zu den Einzelnen Elektronen Eines Atoms," *Physica*, vol. 1, no. 1–6, pp. 104–113, Jan. 1934.

[34] T. Lu and F. Chen, "Multiwfn: A multifunctional wavefunction analyzer," *J. Comput. Chem.*, vol. 33, no. 5, pp. 580–592, 2012.

[35] W. Humphrey, A. Dalke, and K. Schulten, "VMD: Visual molecular dynamics," *J. Mol. Graph.*, vol. 14, no. 1, pp. 33–38, 1996.

[36] T. Yanai, D. P. Tew, and N. C. Handy, "A new hybrid exchange–correlation functional using the Coulomb-attenuating method (CAM-B3LYP)," *Chem. Phys. Lett.*, vol. 393, no. 1, pp. 51–57, 2004.